Eur. Phys. J. Special Topics **227**, 1063–1076 (2018)

https://doi.org/10.1140/epjst/e2018-800080-6

THE EUROPEAN PHYSICAL JOURNAL SPECIAL TOPICS

Regular Article

Stimulus-evoked activity in clustered networks of stochastic rate-based neurons

Igor Franović[1,a] and Vladimir Klinshov[2,b]

[1] Scientific Computing Laboratory, Center for the Study of Complex Systems, Institute of Physics Belgrade, University of Belgrade, Pregrevica 118, 11080 Belgrade, Serbia
[2] Institute of Applied Physics of the Russian Academy of Sciences, 46 Ulyanov Street, 603950 Nizhny Novgorod, Russia

Received 29 April 2018 / Received in final form 22 June 2018
Published online 12 December 2018

Abstract. Understanding the effect of network connectivity patterns on the relation between the spontaneous and the stimulus-evoked network activity has become one of the outstanding issues in neuroscience. We address this problem by considering a clustered network of stochastic rate-based neurons influenced by external and intrinsic noise. The bifurcation analysis of an effective model of network dynamics, comprised of coupled mean-field models representing each of the clusters, is used to gain insight into the structure of metastable states characterizing the spontaneous and the induced dynamics. We show that the induced dynamics strongly depends on whether the excitation is aimed at a certain cluster or the same fraction of randomly selected units, whereby the targeted stimulation reduces macroscopic variability by biasing the network toward a particular collective state. The immediate effect of clustering on the induced dynamics is established by comparing the excitation rates of a clustered and a homogeneous random network.

1 Introduction

Characterizing the structure of spontaneous emergent activity in neuronal populations, and the fashion in which it is modulated by the sensory stimuli, is fundamental to understanding the principles of information processing in the cortex. The generic patterns of spontaneous cortical dynamics, called slow rate fluctuations or UP–DOWN states, involve switching between the episodes of elevated neuronal and synaptic activity, and the stages of relative quiescence [1–3]. Alternation between UP and DOWN states is orchestrated by coherent action of individual neurons, with the observed rates typically lying in the range from 0.1 to 2 Hz [3]. Slow rate fluctuations give rise to macroscopic variability in the cortex [4,5], underlying in vivo activity during quiet wakefulness, sleep or under anesthesia [1,6,7], and even featuring in various in vitro preparations [8,9]. Our paper focuses on the open issues concerning the ingredients that affect the relationship between the stimulus-evoked and the ongoing

[a] e-mail: franovic@ipb.ac.rs
[b] e-mail: vladimir.klinshov@ipfran.ru

dynamics of neural assemblies, as well as the way the induced activity depends on the stimulus.

The research on induced patterns in sensory cortical areas has surprisingly shown that regardless of the type of stimuli, these patterns exhibit remarkable similarity to those of the idling activity [10–13]. In fact, the onset of UP–DOWN states has been recorded while performing perceptual tasks, but has also been found crucial to pyramidal neurons of neocortex, where it facilitates certain forms of learning and memory consolidation [1,14–17]. Such data evince that typical evoked activity patterns are drawn from a limited "vocabulary" already present within the spontaneous dynamics [10], whereby the sampling ability is pinned by the form of sensory stimuli. The striking similarity between the ongoing and the induced cortical activity is now considered as a generic feature of cortical dynamics, verified at increasing levels of structural complexity [18]. Certain experimental studies have linked the similarity to nontrivial properties of cortical connectivity, suggesting that it confines the pool of potential activity patterns [18]. By this paradigm, the structure of patterns reflects the modular (clustered) architecture of cortical networks, whereby certain patterns are activated by stimulating particular local subcircuits, known as the leader sites [19]. Conceptually, investigating the impact of clustered topology on different aspects of collective dynamics is biologically plausible [5,20], as recent research indicates strong prevalence of clustered over the homogeneous connectivity in cortical networks [21–24]. Clustering has already been shown to enable task-specialization, maintaining of high levels of neuronal activity, or adaptation to certain types of stimuli [25,26].

Here, we examine how the interplay of modular network architecture and noise influences the relation between the spontaneous and induced macroscopic activity, as well as how the macroscopic variability is affected by the different types of network stimulation. We analyze a model of a clustered network of noisy rate-based neurons [27–29], employing a second-order effective model of collective dynamics to gain insight into the structure of network's metastable states. While the spontaneous activity consists of noise-induced fluctuations between the metastable states, we show that the specific type of stimulation, targeted at a certain cluster, biases the network toward a particular state, thereby reducing the macroscopic variability.

The origin of macroscopic variability, as an emergent network phenomenon, has so far been treated within two different frameworks, one associating slow rate fluctuations to deterministic networks, where balanced massive excitation and inhibition render the collective dynamics highly sensitive to fluctuations, and the other, which ties the slow rate fluctuations to multistability in attractor model networks, such that switching between coexisting states emerges due to noise, whose action amounts to a finite-size effect. In our recent paper [27], we have applied the latter approach, comparing the switching dynamics in clustered networks relative to random (statistically uniform) networks with the same average connectivity, having shown that clustering promotes multistability, thereby enhancing the switching phenomenon and its robustness. Here, the use of effective model of collective dynamics derived in [27] is extended to capture the response of random and clustered networks to external stimuli. In case of clustered networks, we compare the effects of two different stimulation protocols, including (i) the targeted stimulation, where an increased bias current is introduced only to units in a certain cluster, and (ii) the distributed stimulation, where the same fraction of randomly selected neurons is excited. It is found that due to modular architecture, the two stimulation scenarios may give rise to fundamentally different responses of the network.

The paper is organized as follows. In Section 2, we introduce the model of network dynamics and present the effective model of its macroscopic behavior. Section 3 contains the bifurcation analysis of the effective model of a clustered network in

the thermodynamic limit, applying it to anticipate the induced dynamics of the network. In Section 4, we compare the numerical results to the predictions of the mean-field model. Section 5 provides a brief summary and discussion on the obtained results.

2 Network dynamics: full and the effective model

We consider an m-cluster network comprised of N neurons, assuming random connectivity both within and between the clusters. The intra-cluster connectivity, specified by connectedness probability p_{in}, is more dense than the cross-connectivity p_{out}, whereby the degree of topological heterogeneity is characterized by the clustering parameter $g = p_{\text{in}}/p_{\text{out}}$. Larger g implies stronger clustering, such that the limiting case $g = 1$ describes the non-clustered (homogeneous random) network, while the case $g \to \infty$ corresponds to a network of uncoupled clusters. The clustering algorithm involves rewiring of a sparse random network, and thus preserves the average connectedness probability, set to a biologically plausible level $p = 0.2$. The parameters p_{in} and p_{out} can be linked to p via $p_{\text{in}} = \frac{gm}{m-1+g}p$ and $p_{\text{out}} = \frac{m}{m-1+g}p$, which allows one to explicitly compare the relevant parameter domains between the homogeneous and the clustered network.

The local dynamics follows a stochastic rate model [27–31]

$$\frac{dr_{Xi}}{dt} = -\lambda_X r_{Xi} + H(v_{Xi}) + \sqrt{2D}\xi_{Xi}(t), \tag{1}$$

where r_{Xi} is the firing rate of neuron i from cluster X, λ_X defines the rates relaxation time, and H is the nonlinear gain function, whose argument is the total input to a neuron v_{Xi}. The latter is given by $v_{Xi} = u_{Xi} + I_X + \sqrt{2B}\eta_{Xi}(t)$, where u_{Xi} is the synaptic input $u_{Xi} = \kappa \sum_Y \sum_j a_{YXji} r_{Yj}$ and I_X denotes the external bias current. The coupling scheme is specified by the adjacency matrix $a_{YXji} \in \{0, 1\}$, such that a_{YXji} stands for the link projecting from neuron j in cluster Y to neuron i in cluster X. Coupling weights are assumed to be homogeneous and scale with the network size as $\kappa = K_{YX}/N$. The random perturbations in the microscopic dynamics derive from two distinct sources of noise. In particular, the external noise, characterized by B, and the intrinsic noise, described by D, are introduced to account for the action of synaptic and ion-channel noise, respectively. All the associated fluctuations are independent and are given by Gaussian white noise.

Note that the form (1) is quite general, in a sense that by choosing different H, one may interpolate between different classes of models, including Wilson–Cowan or Hopfield model. From a broader perspective, a plausible gain function should meet three simple requirements: it should drop to zero for sufficiently small input, exhibit saturation for large enough input, and just be monotonous for intermediate input values. Here, the form of H

$$\mathcal{H}(U) = \begin{cases} 0, & U \leq 0, \\ 3U^2 - 2U^3, & 0 < U < 1, \\ 1, & U \geq 1. \end{cases} \tag{2}$$

is selected to make the analysis of macroscopic dynamics analytically tractable [27–29]. Note that the qualitative physical picture associated to the collective multistable behavior in assemblies of neurons with rate-based dynamics does not depend

on the particular choice of the gain function. This point has been extensively elaborated in [30], and we have also numerically verified that the results presented here persist for the Heaviside-like gain function.

2.1 Effective model of clustered network dynamics

The effective model of network dynamics is comprised of coupled mean-field models representing the activities of particular clusters. Typically, the effective models of network behavior concern either the case of random sparse connectivity or the case of full connectivity. In this context, our model can be seen as interpolating between the two standard scenarios, featuring dense intra-cluster connectivity and sparse inter-cluster connections. The applied mean-field approach involves a Gaussian closure hypothesis [32–35], such that the collective dynamics of each cluster X is described by the mean-rate R_X and the associated variance S_X

$$R_X = \frac{1}{N_X}\sum_i r_{Xi} \equiv \left\langle r_{Xi} \right\rangle S_X = \left\langle r_{Xi}^2 \right\rangle - R_X^2, \tag{3}$$

where $\langle\cdot\rangle$ denotes averaging over the neurons within the given cluster. For each of the clusters, we use the bottom-up approach to obtain the second-order stochastic equations of macroscopic behavior. With the detailed derivation of the effective model already provided in [27], here we only briefly outline the two main steps necessary to carry out the appropriate averaging over the microscopic dynamics, namely the Ansatz on local variables and the Taylor expansion of $\mathcal{H}$ function.

The Ansatz on local variables consists in writing r_{Xi} as $r_{Xi} = R_X + \sqrt{S_X}\rho_{Xi}$ [36], where $\{\rho_{Xi}\}$ is a set of variables satisfying $\langle\rho_{Xi}\rangle = 0, \langle\rho_{Xi}^2\rangle = 1$, as readily follows from definition (3). The introduced Ansatz is applied to rewrite the total input to a neuron as $v_{xi} = U_X + \delta v_{Xi}$, where

$$U_X = I_X + \kappa\sum_Y p_{YX}N_Y R_Y \tag{4}$$

presents the assembly-averaged input to cluster X, p_{YX} denotes the connectedness probability from cluster Y to cluster X, and N_Y is the size of cluster Y. The deviation δv_{Xi} from the average input U_X consists of two terms:

$$\delta v_{Xi} = \kappa\sum_Y R_Y\nu_{YXi} + \kappa\sum_Y \sqrt{S_Y}\sigma_{YXi}. \tag{5}$$

The first term accounts for the topological effect associated to the deviation $\nu_{YXi} = \sum_j a_{YXji} - p_{YX}N_Y$ from the average number of connections $p_{YX}N_Y$, whereas the second term captures the effect of local rate fluctuations, contained within the factor $\sigma_{YXi} = \sum_j a_{YXji}\rho_{Yj}$. Equations (4) and (5) allow one to average the terms containing the gain function by developing $H(v_{Xi})$ about U_X up to second order. This leads to $H(v_{Xi}) = H_{0X} + H_{1X}\delta v_{Xi} + H_{2X}\delta v_{Xi}^2$, having introduced notation $H_{0X} \equiv H(U_X), H_{1X} = \frac{dH}{dv_{Xi}}(U_X), H_{2X} = \frac{1}{2}\frac{d^2H}{dv_{Xi}^2}(U_X)$.

Following a number of intermediate steps elaborated in [27], one arrives at the effective model of network dynamics stated in terms of interacting finite-size mean-field models describing the cluster dynamics. The effective model is given by

$$\begin{aligned}\frac{dR_X}{dt} &= -\lambda_X R_X + H_{0X} + 2B_X H_{2X} + H_{2X}\sum_Y K_{YX}^2 p_{YX} N_Y \left(R_Y^2 + S_Y\right)\Big/ N^2 \\ &\quad + \sqrt{\Psi_X}\beta(t) + \sqrt{\Omega_X}\eta, \\ \frac{dS_X}{dt} &= -2\lambda_X S_X + 2B_X H_{1X}^2 + 2D_X, \end{aligned} \tag{6}$$

and involves three types of finite-size effects, including the small deterministic correction term, the effective "macroscopic" noise of intensity Ψ_X, as well as the quenched randomness, accounting for the fact that each particular network realization features distinct deviations from the average connectivity degree. The macroscopic noise is multiplicative

$$\Psi_X = \frac{1}{N}\left(2D_X + 2B_X H_{1X}^2\right) + \frac{1}{N}H_{1X}^2 \sum_Y K_{YX}^2 p_{YX}\frac{N_Y}{N_X}S_Y, \tag{7}$$

and incorporates three terms: the first two describe how the local external and intrinsic noise are translated to macroscopic level, whereas the third one reflects the impact of local fluctuations in the input arriving to each neuron in the cluster. At variance with the time-varying stochastic term featuring $\beta(t)$, the effect of quenched randomness in (6) is characterized by a constant random term of magnitude $\Omega_X = \frac{1}{N}H_{1X}^2 \sum\limits_Y K_{YX}^2 p_{YX}\frac{N_Y}{N_X}R_Y^2$, with η being just a constant random number $\mathcal{N}(0,1)$.

In the S_X dynamics, for simplicity we omit all the finite-size effects, including the deterministic correction and the stochastic terms. One may do so because the variance S_X only affects the $\mathcal{O}(1/N)$ terms in the dynamics of R_X.

3 Bifurcation analysis of the effective model in the thermodynamic limit

In this section, we carry out the bifurcation analysis of the system (6) in the limit $N \to \infty$ to characterize the response of a clustered network to external stimuli. Our focus is on the scenario of targeted stimulation, where an increased bias current is applied to a certain cluster, while the rest of the network remains unperturbed. The stimulation is provided in the form of a rectangular pulse, whose duration Δ is sufficiently long such that the network is allowed to reach the new metastable state. Our analysis will address the issues of why the evoked states of the network are similar to those occurring within the spontaneous activity, and how the stimulus biases the network dynamics to a particular collective state. Note that the system (6) holds for networks of an arbitrary number of clusters of arbitrary sizes, but for simplicity we consider the case of m equal clusters of size $N_c = N/m$.

In our previous study, the model (6) has been analyzed in case where the entire network receives homogeneous external current I. Here, we deal with inhomogeneous stimulation, conforming to a paradigm with l clusters delivered the current I_A, whereas the remaining ones are influenced by I_B. One is interested into solutions where the mean activity of the unperturbed clusters equals R_B, whereas the state of

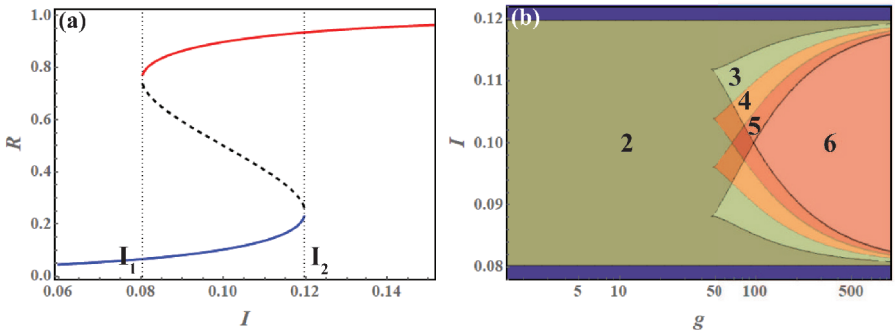

Fig. 1. (a) Bifurcation diagram $R(I)$ for the non-clustered network subjected to homogeneous stimulation. The network parameters are $\alpha = 0.8$, $B = 0.004$, $D = 0.02$ and $g = 1$. (b) Bifurcation diagram for the clustered network $m = 5$ influenced by the homogeneous stimulation: bias current I against logarithm of the clustering coefficient g. The numbers indicate how many coexisting attractors exist within the given region.

the excited clusters R_A may be different. Neglecting the finite-size effects $\mathcal{O}(1/N)$, it follows that the network dynamics is given by

$$\begin{aligned}\frac{dR_A}{dt} &= -R_A - 2U_A\Big(R_A, R_B\Big)^3 + 3U_A\Big(R_A, R_B\Big)^2 + 6B\Big(1 - 2U_A\Big(R_A, R_B\Big)\Big)\\ \frac{dR_B}{dt} &= -R_B - 2U_B\Big(R_A, R_B\Big)^3 + 3U_B\Big(R_A, R_B\Big)^2 + 6B\Big(1 - 2U_B\Big(R_A, R_B\Big)\Big),\end{aligned} \quad (8)$$

where the average input to the two subsets of clusters reads

$$\begin{aligned}U_A\Big(R_A, R_B\Big) &= I_A + \frac{\alpha}{m - 1 + g}\Big[\Big(g + l - 1\Big)R_A + \Big(m - l\Big)R_B\Big]\\ U_B\Big(R_A, R_B\Big) &= I_B + \frac{\alpha}{m - 1 + g}\Big[lR_A + \Big(g + m - l - 1\Big)R_B\Big],\end{aligned} \quad (9)$$

having $\alpha = Kp$ denote the network coupling parameter.

Prior to analyzing the induced dynamics of the network, let us briefly consider the spontaneous activity, which is in this framework represented by a setup with homogeneous bias currents $I_A = I_B = I$. In case of a non-clustered network ($g = 1$), one observes bistability in a certain interval $I \in [I_1, I_2]$ [29], provided the coupling parameter α is sufficiently large. The corresponding bifurcation diagram $R(\alpha)$ in Figure 1a contains two stable branches associated to the UP and DOWN states of the network. Introducing sufficiently strong clustering promotes multistability, giving rise to network states which do not exist in the non-clustered case. The increased number of network levels derives from the states with broken symmetry, where subsets of clusters may lie in their respective high or low states [27]. For such inhomogeneous collective states, the system symmetry is reduced from the permutation group Σ_m (permutation of all cluster indices), to a subgroup of the type $\Sigma_l \otimes \Sigma_{m-l}$, where $l \in \{1, 2, , m - 1\}$. Given that each cluster may either lie in the low or the high state, the maximal multistability of a network comprised of m clusters is $m + 1$. To provide an example, in Figure 1b is shown a bifurcation diagram in the (g, I) plane for a modular network $m = 5$. There, one observes that maximal multistability is facilitated by the clustering parameter $g \gtrapprox 100$.

Note that the external noise B acts in (8) as a bifurcation parameter, influencing the number and position of stationary states in the thermodynamic limit. Figure 2a

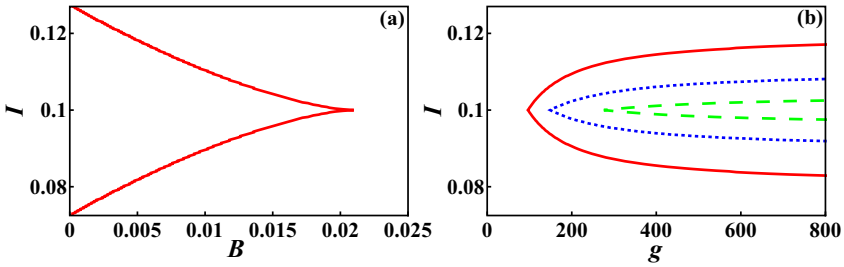

Fig. 2. (a) Bifurcation diagram in the (B, I) for the non-clustered network subjected to homogeneous stimulation. The remaining parameters are $\alpha = 0.8$, $D = 0.02$ and $g = 1$. (b) Shift of the maximal multistability region in the (g, I) plane for a clustered network $m = 5$. The red solid lines outline the maximal multistability domain for noise level $B = 0.004$, whereas the blue dotted lines and the green dashed lines correspond to $B = 0.01$ and $B = 0.015$, respectively.

shows the bifurcation diagram referring to spontaneous activity of the non-clustered network in the (B, I) plane, obtained under fixed connectivity $\alpha = 0.8$. The bistability region again lies between two branches of fold bifurcations (red curves) that meet at the cusp point, where a pitchfork bifurcation occurs. One finds that for fixed I, there always exists a B value above which a non-clustered network can no longer support bistable behavior. For the spontaneous dynamics of a clustered network, it can be shown that the region of maximal multistability in the (g, I) plane, bounded by two curves of fold bifurcations intersecting at the pitchfork bifurcation, reduces and shifts toward stronger clustering under increasing B, cf. Figure 2b. In other words, for higher external noise, one requires larger clustering in order to observe maximal multistability in the network.

To investigate the scenario of a targeted stimulation, we analyze the network's response by looking into solutions of (8) for $l = 1$, such that the stimulated cluster occupies the state different from the remaining clusters. The clustering coefficient g and the stimulation current I_A are considered as control parameters, while the remaining parameters $\alpha = 0.8$, $B = 0.004$, and $I_B = 0.1$ are such that the spontaneous dynamics of the associated homogeneous random network with $I = I_B$ pertains to bistability region in Figure 1a. The (g, I_A) bifurcation diagram explaining the action of targeted stimulation is plotted in Figure 3a. For $I_A \approx I_B$ and strong enough clustering, the network possesses four stable steady states, which can readily be traced in the limit of ultimate clustering $g \to \infty$. Indeed, suppose that a network is decomposed into a set of non-interacting clusters, and that I_A and I_B lie within the interval $[I_1, I_2]$ from Figure 1a. Then, each of the clusters is bistable, which gives exactly four stable steady states in the full system (8). The area of maximal multistability, where both the stimulated cluster and the resting network may either occupy the low or the high state, extends to moderate clustering $g \sim 100$. In Figure 3b, the four stable steady states of the effective model are denoted by O_{LL}, O_{LH}, O_{HL} and O_{HH}. Note that the first and second index refer to states of the stimulated cluster and the rest of the network, respectively, whereby L/H indicates the low/high level, and U denotes the unstable state.

As the stimulation I_A increases, the system undergoes a saddle-node bifurcation in which the states O_{LH} and O_{UH} are annihilated, see the curve C_1 in Figure 3a. Then the system passes to the area with 3 stable steady states, with the corresponding phase portrait shown in Figure 3c. Further growth of I_A causes the states O_{LL} and O_{UL} to collide, cf. the curve C_2 in Figure 3a, such that the system becomes bistable, as corroborated by the phase portrait in Figure 3d. For small g, very strong simulation I_A leads to a collision and disappearance of the steady states O_{HL}

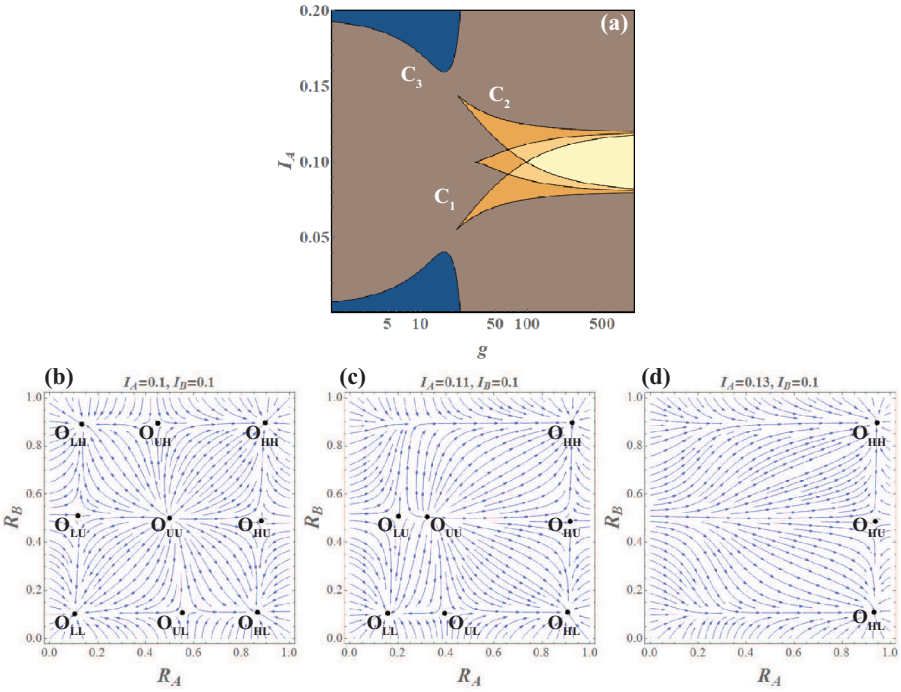

Fig. 3. (a) Bifurcation diagram $I_A(g)$ of system (8), with the number of coexisting solutions indicated for particular regions. The remaining parameters are fixed to $\alpha = 0.8$, $B = 0.004$, $D = 0.02$, $m = 5$ and $I_B = 0.1$. (b–d) Phase portraits associated to system (8) under increasing I_A.

and O_{HU}, see the curve C_3 in Figure 3a, whereby the system becomes monostable. Note that the decrease of I_A (targeted inhibition) gives rise to a similar scenario. When I_A is systematically reduced, the system first becomes tristable with coexisting states O_{LL}, O_{LH} and O_{HH}, then bistable and eventually passes to monostability domains.

4 Numerical results: targeted vs. distributed stimulation

In this section, our aim is to first explicitly demonstrate that the effective model (8) can successfully predict the response of a clustered network in case of targeted stimulation. Nevertheless, we shall also show an interesting effect evincing that the response of modular networks to external stimulation is strongly dependent on the character of stimulation, i.e. the fashion in which it is distributed to neurons within the network.

In Figure 4, the response of a clustered network $m = 5$ to a targeted stimulation is compared against the induced dynamics of the effective model analyzed in Section 3. Note that the numerical experiments concerning the full system (1) have been carried out on a relatively small network comprised of $N = 300$ neurons, which corresponds to only 60 neurons per cluster, having fixed the noise levels to $D = 0.02$ and $B = 0.004$. Given the relatively small cluster size, one would expect strong fluctuations in the network dynamics. Nevertheless, it will be shown that even under such conditions, the mean-field analysis performed in case of thermodynamic limit still remains qualitatively valid, in a sense of being able to qualitatively capture the induced behavior of the network.

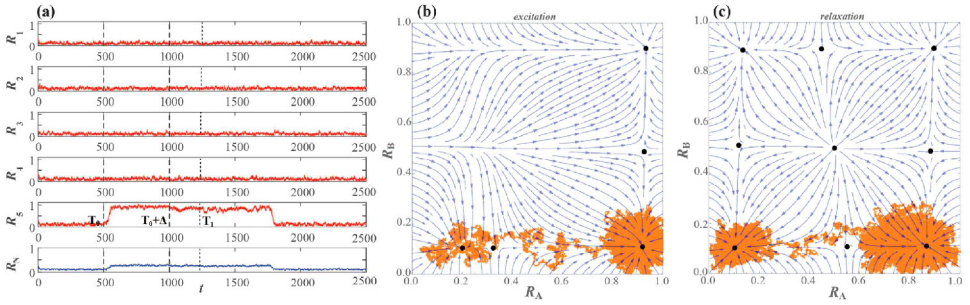

Fig. 4. (a) Response of a clustered network ($m = 5$) to a stimulus of intensity I_A and duration Δ introduced to cluster 5 at the moment T_0. Notation $R_i, i \in [1, 5]$ refers to mean-rates of particular clusters, whereas R_N stands for the collective network activity. Panels (b) and (c) show excitation and relaxation processes of the network in the (R_A, R_B) plane, respectively. The system's orbit is superimposed on the vector field of the effective model (8), obtained for $(I_A, I_B) = (0.12, 0.1)$ in (b) and $I_A = I_B = 0.1$ in (c). The remaining parameters are $g = 250, B = 0.004, D = 0.02$.

The scenario of targeted stimulation unfolds in such a way that before introducing the stimulation, all the clusters occupy the low state and are influenced by the same current $I_A = I_B = 0.1$. Then, at the moment $T_0 = 500$, a rectangular pulse of elevated bias current $I_A = 0.12$ is introduced solely to cluster 5. The pulse is maintained for a sufficiently long time $\Delta = 500$, such that the network is allowed to reach the new metastable state. Note that during the stimulation, I_A lies very close to the bifurcation curve C_2 from Figure 3a. Therefore the state O_{LL} is weakly stable, and the finite-size fluctuations may easily drive the system away from it, as indicated by the time traces in Figure 4a. In Figure 4b, we have plotted the excitation orbit of the network in the (R_A, R_B) plane in order to demonstrate that the system switches between the metastable states anticipated by the effective model (8). In particular, the vector field provided in the background presents the flow of system (8) for $(I_A, I_B) = (0.12, 0.1)$. One observes that the network rapidly leaves the vicinity of the state O_{LL} and switches to O_{HL}, conforming to the path where a single cluster, described by R_A, is perturbed by the stimulation, whereas the remaining clusters, associated to R_B, remain unaffected.

We have also examined the relaxation process of the network after the termination of the stimulus at $t = T_0 + \Delta$. In Figure 4c, the relaxation orbit is plotted against the vector field of the system (8) for $I_A = I_B = 0.1$. As predicted by the effective model, the state O_{HL} lies far from bifurcations, which makes it relatively stable, in a sense that the network may spend quite a long time in its vicinity. However, the fluctuations induced by the finite-size effect eventually drive the network back to the homogeneous DOWN state O_{LL}.

The dependence of the networks response on the stimulation magnitude I_A is illustrated in Figure 5. The response is characterized by the "excitation rate" γ, defined as the average fraction of excited neurons at the moment $T_0 + \Delta$ just after the stimulus has ceased, having performed averaging over an ensemble of 80 stochastic realizations. Since the targeted stimulation may only give rise to excitation of a single cluster, γ in this case is merely the probability of cluster excitation. The response function $\gamma(I_A)$ exhibits threshold-like behavior, with the rising stage triggered at $I_A \approx 0.11$ and completed at $I_A \approx 0.12$, cf. the blue solid line with empty circles. Note that the latter value is in perfect agreement with the prediction of the bifurcation diagram in Figure 3a. For large I_A, the excitation rate saturates at $\gamma = 1/m = 0.2$, which implies that only a single cluster is excited regardless of how large I_A becomes.

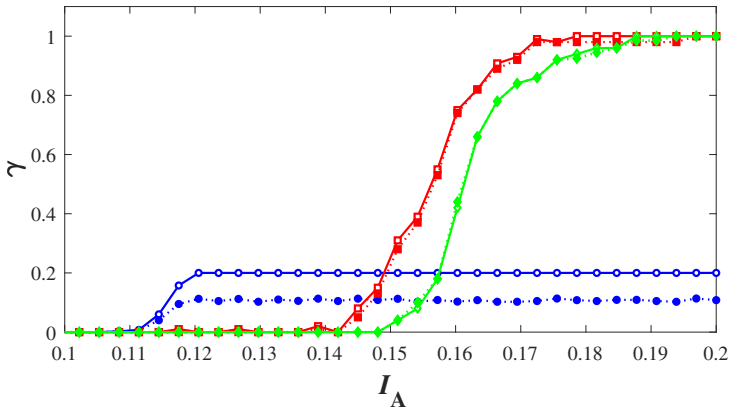

Fig. 5. Excitation rate, i.e. fraction of excited clusters γ in terms of I_A for the different stimulation scenarios. The circles and squares refer to targeted and distributed stimulation of a clustered network ($m = 5, g = 250$), respectively, whereas the diamonds indicate the response of a homogeneous random network ($g = 1$). The empty symbols connected by solid lines denote γ values at the moment $T_0 + \Delta$ when the stimulation is terminated. The solid symbols connected by the dotted lines show γ at the moment T_1 after the stimulation has ceased, cf. Figure 4a. The remaining network parameters are $B = 0.004$, $D = 0.02$ and $I_B = 0.1$.

In general, the persistence of the elevated state does not depend on the applied stimulation magnitude I_A, but is rather determined by the relaxation speed of the state the network occupies at the moment $T_0 + \Delta$ when the stimulation is terminated. In order to analyze the features of the relaxation process, we have measured the excitation rate γ at a later moment $T_1 = 1250$, sufficiently long after the excitation pulse has ceased, cf. the blue dotted line connecting the filled circles in Figure 5. Since in the case of targeted stimulation one always encounters the same excited state with only a single cluster perturbed, it is natural to expect proportionality between the excitation rate immediately after the stimulation (moment $T_0 + \Delta$) and at a later moment T_1. Our results corroborate that the elevated state may indeed persist considerably longer than the triggering pulse.

As already announced, we also report on an interesting finding that the induced dynamics of modular networks strongly depends on the applied stimulation protocol. In particular, suppose that instead of a targeted stimulation, one introduces an elevated bias current to the same fraction of neurons as in a single cluster, but just randomly distributed over the network. We refer to such a scenario as "distributed stimulation". In this instance, for sufficiently large stimulation I_A, the network may reach states where substantially more than a single cluster is elicited, in spite of relatively large clustering coefficient g.

The network excitation rate as a function of I_A for the case of distributed stimulation is indicated by the solid red line with empty squares in Figure 5. One immediately realizes that the impact of the distributed stimulation is quite distinct from that of the targeted one in two aspects: (i) the I_A threshold where it starts to excite a single cluster is significantly larger than for the targeted stimulation and (ii) for sufficiently strong stimulation I_A, all the clusters may cross to high state.

To gain a deeper insight into how the network's response is shaped by clustering, we consider an additional scenario, where a certain fraction of neurons is stimulated in a homogeneous random network $g = 1$. To allow the comparison, we have perturbed the same fraction of units as in the clustered network, but here one cannot distinguish between the targeted and the distributed stimulation protocols

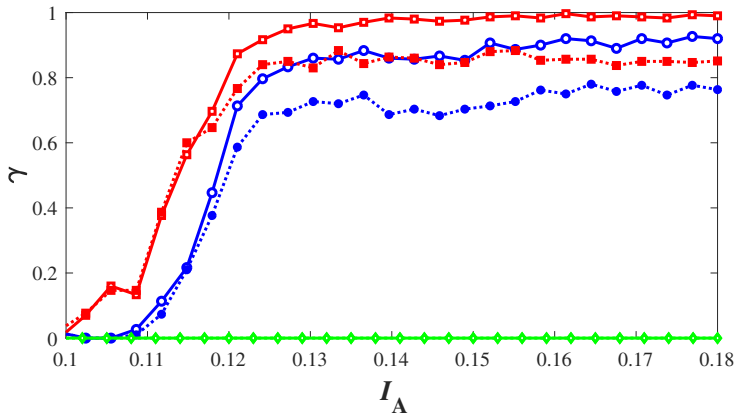

Fig. 6. Dependence of excitation rate γ on the applied current I_A for levels of external noise B where the network cannot exhibit maximal multistability. The green diamonds concern the response of a homogeneous random network $g = 1$ in case where the effective model exhibits only the DOWN state ($B = 0.028, D = 0.02, I_B = 0.1$). The blue circles and the red squares refer cases of a targeted and distributed stimulation of a clustered network $m = 5$, respectively. In the thermodynamic limit, the parameters of the clustered network facilitate bistable dynamics between the homogeneous UP and DOWN states ($B = 0.018, D = 0.02, g = 60, I_B = 0.1$). The solid/empty symbols are used the same way as in Figure 5.

because any subset of units is equivalent. The ensuing excitation rate, plotted in Figure 5 by the solid green line, indicates a response substantially distinct from that of a clustered network in case of targeted stimulation, but reminiscent of the induced dynamics typical for the distributed stimulation. This is so because the homogeneous network possesses only two metastable states, namely the homogeneous DOWN and UP states, which implies that one cannot excite only a certain fraction of units, but can rather excite the entire network. As the DOWN state vanishes at the bifurcation curve C_3 in Figure 3a, the guaranteed excitation of the network is observed only if I_A lies sufficiently close to this curve. The associated threshold current corresponds to the saturation of the excitation rate observed at $I_A \approx 0.19$ in Figure 5.

As already indicated, the external noise influences the multistable dynamics of both the homogeneous and the clustered networks. In Figure 6, it is examined how the excitation rate changes if the level of external noise B is increased such that the network can no longer exhibit maximal multistability in the thermodynamic limit. For the non-clustered network, we have considered the case where the deterministic dynamics is monostable, admitting only the DOWN state. As expected, stimulating a fraction of neurons with arbitrary strong external current cannot switch the network to the UP state, cf. the green diamonds in Figure 6. For the clustered network $m = 5$, the external noise B and the clustering coefficient g have been set such that the deterministic dynamics exhibits only bistability between the homogeneous UP and DOWN states. For both the scenarios of the targeted and distributed stimulation protocols, the excitation rate exhibits a threshold-like behavior, ultimately reaching the network-wide UP state for a sufficiently strong stimulation. As predicted by the effective model, the targeted stimulation can no longer bring the network to a heterogeneous state where only a single cluster is excited.

5 Summary and discussion

In the present paper, we have analyzed the induced dynamics of a clustered network subjected to two types of stimulation protocols, the targeted stimulation and the distributed stimulation. In the former case, it has explicitly been demonstrated that the effective model, describing the macroscopic dynamics in terms of coupled mean-field models associated to each of the clusters, may accurately capture the networks response, predicting the metastable state reached by the network.

An interesting finding is that the response of a clustered network strongly depends on the applied stimulation protocol. In particular, in case of a targeted stimulation, under sufficiently strong clustering, one typically observes that only the targeted cluster is activated, whereas the remaining clusters are unaffected by the perturbation. Nevertheless, for the distributed stimulation, applying a sufficiently strong excitation may result in much richer dynamics, where different forms of elevated states, including a network-wide high state, may be reached.

Concerning the immediate impact of the modular network architecture, we have established that the response of a clustered network is drastically different from that of a statistically homogeneous one even if the same number of randomly selected units is stimulated. In particular, given the same stimulation magnitude, the excitation rate of the homogeneous random network turns out to be substantially lower than that of a clustered network. This distinction derives from the fact that a non-clustered network cannot exhibit heterogeneous states. As expected, the differences in behavior of the non-clustered and clustered networks vanish for sufficiently strong stimuli, where the network-wide excitation becomes the prevalent scenario regardless of the network structure. In case of a non-clustered network, the reduced model has been shown to provide a good estimate of the threshold current that guarantees reaching the elevated state.

The external noise has been found to play a nontrivial role with respect to the excitation process, because it affects the features of the network's multistable behavior in the thermodynamic limit. This is a consequence of the fact that the macroscopic noise derived from the local external noise is multiplicative [37]. The associated changes in the multistability have been shown to substantially influence the excitation rates in clustered networks for both the stimulation protocols, as well as in the scenario where the stimulus acts on a certain fraction of neurons in a non-clustered network.

For the particular stimulation protocol, the properties of the relaxation process are found not to be determined by the intensity of excitation, but rather by the state of the network at the moment the stimulation is terminated. One should note that instances of prolonged relaxation have been observed, especially in the case of distributed stimulation under higher intensities of the applied current, which facilitate excitation to the homogeneous UP state. The lifetimes of the metastable states are also influenced by the level of the external noise, and the underlying effects provide an interesting topic for future studies. In particular, the impact of multistability on the relaxation process may consist in inducing nonlinear dependencies of relaxation times on the noise level, which can manifest as noise-enhanced stability of metastable states [38,39].

Within the present study, we have explained by the effective model, and corroborated numerically, why the induced dynamics of a clustered network resembles the spontaneous one, further demonstrating how the stimulation biases the network toward a particular collective state. Recent experimental research indicates that the external stimulation reduces both the macroscopic and the microscopic neuronal variability [10,40,41], the latter being associated to randomness in local dynamics, viz. the spiking series of individual units. While our results may indeed account for the stimulation-induced decrease of macroscopic variability, one cannot

infer anything regarding the microscopic variability, since we apply a rate-based neuron model. In this context, it would be of interest to consider in detail the induced dynamics of a clustered network of spiking neurons via an effective model, especially given that the numerical results in [5,13,20] already link the stimulated activity with reduction of both the macroscopic and microscopic neuronal variability.

This work is supported by the Ministry of Education, Science and Technological Development of Republic of Serbia under project No. 171017, by the Russian Foundation for Basic Research under project No. 17-02-00904, and by the Russian Science Foundation under project No. 16-42-01043.

References

1. T.T.G. Hahn, J.M. McFarland, S. Berberich, B. Sakmann, M.R. Mehta, Nat. Neurosci. **15**, 1531 (2012)
2. G. Buzsáki, C.A. Anastassiou, C. Koch, Nat. Rev. Neurosci. **13**, 407 (2012)
3. V.V. Vyazovskiy, K.D. Harris, Nat. Rev. Neurosci. **14**, 443 (2013)
4. M.R. Cohen, A. Kohn, Nat. Neurosci. **14**, 811 (2011)
5. A. Litwin-Kumar, B. Doiron, Nat. Neurosci. **15**, 1498 (2012)
6. C.C.H. Petersen, T.T.G. Hahn, M. Mehta, A. Grinvald, B. Sakmann, Proc. Natl. Acad. Sci. U.S.A. **100**, 13638 (2003)
7. D. Millman, S. Mihalas, A. Kirkwood, E. Niebur, Nat. Phys. **6**, 801 (2010)
8. J. Anderson et al., Nat. Neurosci. **3**, 617 (2000)
9. R. Cossart, D. Aronov, R. Yuste, Nature **423**, 283 (2003)
10. A. Luczak, P. Barthó, K.D. Harris, Neuron **62**, 413 (2009)
11. A. Luczak, P. Barthó, K.D. Harris, J. Neurosci. **33**, 1684 (2013)
12. D.L. Ringach, Curr. Opin. Neurobiol. **19**, 439 (2009)
13. G. Deco, E. Hugues, PLoS Comput. Biol. **8**, e1002395 (2012)
14. D. Ji, M.A. Wilson, Nat. Neurosci. **10**, 100 (2007)
15. S. Diekelmann, J. Born, Nat. Rev. Neurosci. **11**, 114 (2010)
16. D. Miyamoto et al., Science **352**, 1315 (2016)
17. G. Rothschild, E. Eban, L.M. Frank, Nat. Neurosci. **20**, 251 (2017)
18. J.L. Vincent et al. Nature **447**, 83 (2007)
19. V. Pasquale, S. Martinoia, M. Chiappalone, Sci. Rep. **7**, 9080 (2017)
20. B. Doiron, A. Litwin-Kumar, Front. Comput. Neurosci. **8**, 56 (2014)
21. S. Song, P. Sjöström, M. Reigl, S. Nelson, D. Chklovskii, PLoS Biol. **3**, e68 (2005)
22. S. Lefort, C. Tomm, J.-C.F. Sarria, C.C.H. Petersen, J.C. Floyd Sarria, C.C.H. Petersen, Neuron **61**, 301 (2009)
23. R. Perin, M. Telefont, H. Markram, Front. Neuroanat. **7**, 1 (2013)
24. V.V. Klinshov, J.N. Teramae, V.I. Nekorkin, T. Fukai, PLoS One **9**, e94292 (2014)
25. S.B. Hofer, H. Ko, B. Pichler, J. Vogelstein, H. Ros et al., Nat. Neurosci. **14**, 1045 (2011)
26. H. Ko, S.B. Hofer, B. Pichler, K.A. Buchanan, P.J. Sjöström, T.D. Mrsic-Flogel, Nature **473**, 87 (2011)
27. I. Franović, V. Klinshov, Chaos **28**, 023111 (2018)
28. I. Franović, V. Klinshov, Europhys. Lett. **116**, 48002 (2016)
29. V. Klinshov, I. Franović, Phys. Rev. E **92**, 062813 (2015)
30. H. Hasegawa, Phys. Rev. E **75**, 051904 (2007)
31. R.A. Anderson, S. Musallam, B. Pesaran, Curr. Opin. Neurobiol. **14**, 720 (2004)
32. B. Lindner, J. Garcia-Ojalvo, A. Neiman, L. Schimansky-Geier, Phys. Rep. **392**, 321 (2004)
33. M.A. Zaks, X. Sailer, L. Schimansky-Geier, A.B. Neiman, Chaos **15**, 026117 (2005)
34. I. Franović, K. Todorović, N. Vasović, N. Burić, Phys. Rev. E **87**, 012922 (2013)

35. I. Franović, K. Todorović, N. Vasović, N. Burić, Phys. Rev. E **89**, 022926 (2014)
36. A.N. Burkitt, Biol. Cybern. **95**, 1 (2006)
37. S. Ciuchi, F. de Pasquale, B. Spagnolo, Phys. Rev. E **47**, 3915 (1993)
38. N.V. Agudov, A.A. Dubkov, B. Spagnolo, Physica A **325**, 144 (2003)
39. G. Augello, D. Valentia, B. Spagnolo, Eur. Phys. J. B **78**, 225 (2010)
40. L. Mazzucato, A. Fontanini, G. La Camera, J. Neurosci. **35**, 8214 (2015)
41. I.-C. Lin, M. Okun, M. Carandini, K.D. Harris, Neuron **87**, 644 (2015)